Non-equilibrium transport of positron and electron swarms in gases and liquids

2010 Plasma Sources Sci. Technol. 19 034001

(http://iopscience.iop.org/0963-0252/19/3/034001)

Plasma Sources Sci. Technol. **19** (2010) 034001 (10pp) doi:10.1088/0963-0252/19/3/034001

Non-equilibrium transport of positron and electron swarms in gases and liquids

R D White[1], **S Dujko**[1,2], **R E Robson**[1,3], **Z Lj Petrović**[2] **and R P McEachran**[3]

[1] ARC Centre for Antimatter-Matter Studies, School of Physical Sciences and Engineering, James Cook University, Townsville 4810, Australia
[2] Institute of Physics, University of Belgrade, PO Box 68, 11080 Zemun, Belgrade, Serbia
[3] ARC Centre for Antimatter-Matter Studies, Research School of Physical Sciences, Australian National University, Canberra 2600, Australia

E-mail: Ronald.White@jcu.edu.au

Received 12 July 2009, in final form 19 October 2009
Published 21 May 2010
Online at stacks.iop.org/PSST/19/034001

Abstract
The transport properties of positron and electron swarms in gases and liquids find application in many and varied fields. In this paper we present a time-dependent multi-term solution of Boltzmann's equation valid for electrons and positrons, and benchmark it against an independent Monte-Carlo simulation where possible. The transport properties of positrons in dilute gaseous and liquid argon are considered and compared. The sensitivity of the macroscopic transport properties to the anisotropic nature of elastic scattering is highlighted. The temporal non-locality of diffusion for electron swarms in gases under the influence of time-dependent electric and magnetic fields is addressed through the consideration of their associated relaxation profiles.

(Some figures in this article are in colour only in the electronic version)

1. Introduction

What is meant by the term 'swarm'? Firstly, it is normally (but not exclusively) used in connection with an ensemble of charged particles, such as electrons, positrons, muons or ions interacting with a background medium comprising gaseous or condensed matter, often under the influence of applied fields. Secondly, the key requirement is that the ensemble is of sufficiently low-density so that (i) mutual interactions between swarm particles can be neglected; (ii) the background medium as a whole remains essentially undisturbed—specifically the distributions of molecular translational and internal states are not modified and (iii) space-charge fields are negligible in comparison with the applied fields. In plasma physics, this is designated as the free diffusion or test particle limit. Whatever the terminology used, the behaviour of the ensemble is determined by (a) collisions between the swarm particles and background molecules; (b) the applied fields and (c) the properties of the background medium, such as temperature, pressure, molecular mass, molecular velocity distribution function and (for a condensed medium) structural properties.

In swarm experiments (b) and (c) can be fixed, and measurements of certain macroscopic properties (transport coefficients) of the swarm can then be unfolded to yield information about (a), specifically collision cross-sections or interaction potentials. Variation of field strength and temperature allows a whole range of energies to be scanned, right down to thermal energies of about 1/40 eV. This forms the basis of what is sometimes called the swarm method for indirect determination of cross-sections [1–4], and complements the direct procedure in which a beam of particles at a fixed energy is scattered from a target. The golden era of swarm experiments occurred to a large extent in the period 1960–1990, during which time much important and unique data were reported in the literature [1–4]. In recent times, however, the number of groups performing swarm measurements has decreased markedly, while ironically the demand for accurate low energy cross-section data, which only swarm experiments can provide, has increased. Beam experiments can fill the gap up to a point, but the low energy regime still remains the preserve of swarm experiments. Further, such studies are needed to test the cross-sections obtained by other means/techniques not only in terms of their

accuracy but also in terms of the completeness. The lack of experimental swarm measurements inhibits this important process. Further suggestions for future swarm experiments are detailed in [3].

There is another side to swarm experiments which is relevant to the modern era: in addition to furnishing experimental data *per se*, the overall programme produced a spin-off in the form of a comprehensive and highly accurate transport theory used to analyse and unfold the swarm data (see the review [5]). This extended the older but now superseded theory of the 1940s and 1950s, as typified, for example, by Allis [6]. That same transport theory is of sufficient generality so that it now finds application in many and varied applications from low-temperature plasmas to high energy particle detectors, positron traps and medical imaging (see the reviews [3, 7–10]), to name just a few examples, and as highlighted in this paper.

The annihilation of a positron and the electron to yield a pair of gamma rays directed back-to-back is a fundamental process routinely used as a tool in a wide variety of fields ranging from material science to medicine, e.g. positron emission tomography (PET) in diagnosing cancer and degenerative brain diseases [11]. Full utilization of these technologies and success in general in anti-matter frontiers is pivotally dependent on an accurate knowledge of the underlying positron physics from scattering processes through transport. For scattering, the development of improved positron trapping systems (Penning–Malmberg–Surko traps) has led to the development of high resolution positron beams which when combined with new scattering techniques enable unparalleled accuracy in the determination of positron impact cross-sections [12, 13], complementing the many advanced *ab initio* calculations [14, 15].

One of the key elements in optimizing positron-based technologies is an understanding of low-density positron transport in gaseous and condensed systems. With the recent availability of accurate positron scattering cross-sections the field of positron swarm transport in dilute gases has recently been revitalized for non-equilibrium systems [16, 17] and in the context of modelling the Penning–Malmberg–Surko traps [18]. The positronium formation process has given rise to new phenomena including Ps-induced negative differential conductivity [16, 17, 19]. While the transport theory of positrons in dilute gaseous systems is fairly well established, there have been limited investigations of positrons in liquids and soft-condensed matter. In a recent study, a multi-term solution of Boltzmann's equation was developed and applied to positrons in liquid argon [19].

For low-temperature plasmas, in contrast to swarms, charge densities are sufficiently high so that space-charge fields, Coulomb collisions and disturbance of the neutral gas may be significant. Importantly, however, there is considerable overlap with the transport theory used in swarm physics. Moreover, the results of swarm studies provide a benchmark in the free diffusion limit of a plasma, and thus more sophisticated/elaborate kinetic, fluid and hybrid theories that model low-temperature plasmas can be validated in this limit. In recent times, various groups (Belgrade group see, e.g., [3, 10, 20–22], JCU group see, e.g., [8, 9, 23–27], Greifswald group see, e.g. [7, 28, 29] and others [30–32]) have focused on the developed Boltzmann equation solutions and MC simulations in the swarm limit, with the aim of understanding the complex kinetic phenomena present for radio frequency (rf). and magnetized plasmas including temporal and spatial non-locality. Further to this, swarm transport data are also used to evaluate collisional transfer rates in fluid and hybrid models. This swarm–plasma nexus has been explored and highlighted in various recent studies [3, 8–10, 33].

We begin this paper with a brief overview of swarm transport theory including a time-dependent multi-term solution of the Boltzmann equation for electric and magnetic fields and the equivalent time-resolved Monte Carlo simulation. We split the applications into two sections, positron and electron swarms. In section 3.1, we apply these techniques to positrons in gaseous argon where we highlight the impact of the elastic differential cross-section on the macroscopic transport properties. Comparisons are made with an independent Monte Carlo simulation where possible. Diffusion processes in liquid argon are then presented where they are compared with the dilute gas-phase results. For electron swarms in section 3.2, we focus on the establishment of benchmarks for electron swarms in rf electric and magnetic fields, through a direct comparison of the time-dependent multi-term Boltzmann equation solution and a time-resolved Monte Carlo simulation. The temporal non-locality of electron swarm transport in rf fields is discussed in terms of transient relaxation profiles.

2. Transport theory

2.1. Transport coefficient definitions

Experimental investigations of swarm behaviour are generally made by sampling charged particle currents or charged particle density $n(\boldsymbol{r}, t)$. The connection between experiment and theory is made through the equation of continuity

$$\frac{\partial n(\boldsymbol{r}, t)}{\partial t} + \nabla \cdot \boldsymbol{\Gamma}(\boldsymbol{r}, t) = S(\boldsymbol{r}, t) \ , \tag{1}$$

where $\boldsymbol{\Gamma}(\boldsymbol{r}, t) = n\langle \boldsymbol{c} \rangle$ is the swarm particle flux and $S(\boldsymbol{r}, t)$ represents the production rate per unit volume per unit time arising from non-conservative collisional processes such as Ps-formation, annihilation, ionization, etc.

In carefully controlled swarm experiments, spatial gradients are designed to be small so that the *hydrodynamic regime* in general prevails, and the space–time dependence can be projected onto the number density [34]. Transport coefficients obtained from swarm experiments in this manner are essentially independent of the geometry of the experiment, since all spatial dependences are accounted for by functionals of $n(\boldsymbol{r}, t)$ which are in turn found through the solution of the diffusion equation. In the hydrodynamic regime the space-time dependence of quantities (e.g. flux, source) is projected out through a density gradient expansion. The flux $\boldsymbol{\Gamma}(\boldsymbol{r}, t)$ and

source term $\boldsymbol{S}(\boldsymbol{r}, t)$ in (1) are expanded as follows:

$$\boldsymbol{\Gamma}(\boldsymbol{r}, t) = \boldsymbol{W}_{\mathrm{F}} n(\boldsymbol{r}, t) - \boldsymbol{D}_{\mathrm{F}} \cdot \nabla n(\boldsymbol{r}, t) + \cdots, \tag{2}$$

$$\boldsymbol{S}(\boldsymbol{r}, t) = S^{(0)} - \boldsymbol{S}^{(1)} \cdot \nabla n(\boldsymbol{r}, t) + \boldsymbol{S}^{(2)} : \nabla\nabla n(\boldsymbol{r}, t) + \cdots, \tag{3}$$

where $\boldsymbol{W}_{\mathrm{F}}$ is the flux drift velocity and $\boldsymbol{D}_{\mathrm{F}}$ is the flux diffusion tensor. Substitution of expansions (3) into the continuity equation (1) yields the diffusion equation

$$\frac{\partial n}{\partial t} + \boldsymbol{W} \cdot \nabla n - \boldsymbol{D} : \nabla\nabla n + \cdots = -Rn, \tag{4}$$

where we define the bulk transport coefficients

$$R = S^{(0)}, \tag{5}$$

$$\boldsymbol{W} = \boldsymbol{W}_{\mathrm{F}} + \boldsymbol{S}^{(1)}, \tag{6}$$

$$\boldsymbol{D} = \boldsymbol{D}_{\mathrm{F}} + \boldsymbol{S}^{(2)}\ . \tag{7}$$

The physical origin of the difference between the two sets of coefficients has long been known and we will refer to it as the TSS (Tagashira–Sakai–Sakamoto) effect [35]. We should highlight that while it is the bulk coefficients, not flux coefficients, which are generally determined in swarm experiments, it is often the flux coefficients that are required in fluid models [9] and hence care must be taken in applying such data.

2.2. Space and time-dependent multi-term solution of the Boltzmann's equation

The behaviour of electron and positron swarms in gases under the influence of electric and magnetic fields is described by the phase-space distribution function $f(\boldsymbol{r}, \boldsymbol{c}, t)$ representing the solution of the Boltzmann equation

$$\frac{\partial f}{\partial t} + \boldsymbol{c} \cdot \nabla f + \frac{q}{m} [\boldsymbol{E} + \boldsymbol{c} \times \boldsymbol{B}] \cdot \frac{\partial f}{\partial \boldsymbol{c}} = -J(f, f_0), \tag{8}$$

where $\boldsymbol{r}$ and $\boldsymbol{c}$ denote the position and velocity co-ordinates, q and m are the charge and mass of the swarm particle and t is the time. The electric and magnetic fields are assumed spatially homogeneous and orthogonal with magnitudes E and B, respectively. Swarm conditions are assumed to apply and $J(f, f_0)$ denotes the rate of change of f due to binary collisions with the neutral molecules. The original Boltzmann collision operator [36] and its semiclassical generalization [37] are used for elastic and inelastic processes, respectively. For ionization we implement the operator detailed in [5] while for particle loss processes we use the direct part only of the Boltzmann collision operator. In what follows, we employ a co-ordinate system in which $q\boldsymbol{E}$ is in the z-direction, while $q\boldsymbol{B}$ is in the y-direction.

2.2.1. Representation of the velocity dependence. The velocity dependence of f is represented in terms of a combined spherical harmonic and Sonine polynomial expansion (Burnett functions):

$$f(\boldsymbol{r}, \boldsymbol{c}, t) = w(\alpha, c) \sum_{\nu=0}^{\infty} \sum_{l=0}^{\infty} \sum_{m=-l}^{l} F(\nu l m | \boldsymbol{r}, \alpha, t) R_{\nu l}(\alpha c) Y_m^{[l]}(\hat{\boldsymbol{c}}), \tag{9}$$

where

$$w(\alpha, c) = \left(\frac{\alpha^2}{2\pi}\right)^{3/2} \exp\left\{\frac{-\alpha^2 c^2}{2}\right\}, \tag{10}$$

$$R_{\nu l}(\alpha c) = N_{\nu l} \left(\frac{\alpha c}{\sqrt{2}}\right)^l S_{l+1/2}^{(\nu)}\left(\frac{\alpha^2 c^2}{2}\right), \tag{11}$$

$$N_{\nu l}^2 = \frac{2\pi^{3/2}\nu!}{\Gamma(\nu + l + 3/2)}, \tag{12}$$

$Y_m^{[l]}(\hat{\boldsymbol{c}})$ are spherical harmonics, $\hat{\boldsymbol{c}}$ denotes the angles of $\boldsymbol{c}$, $S_{l+1/2}^{(\nu)}(\alpha^2 c^2/2)$ are Sonine polynomials and $\alpha^2 = m/kT_b$. The modified Sonine polynomials satisfy the orthonormality relation

$$\int_0^\infty w(\alpha, c) R_{\nu' l'}(\alpha c) R_{\nu l}(\alpha c) c^2 \, \mathrm{d}c = \delta_{\nu'\nu}\delta_{l'l}. \tag{13}$$

The various properties of the moments due to symmetry and reality considerations are outlined in [24].

Using the appropriate orthogonality relations, the following system of coupled differential equations for the moments $F(\nu l m; \boldsymbol{r}, t, \alpha)$ is generated:

$$\begin{aligned}
&\sum_{\nu'=0}^{\infty} \sum_{l'=0}^{\infty} \sum_{m'=-l'}^{l'} \Bigg[\left(\frac{\partial}{\partial t}\delta_{\nu\nu'} + n_0 J_{\nu\nu'}^{l}(\alpha)\right) \delta_{l'l}\delta_{m'm} \\
&\quad + \mathrm{i}\frac{qE}{m}\alpha(l'm10|lm)\langle \nu l||K^{[1]}||\nu' l'\rangle \delta_{m'm} \\
&\quad + \frac{1}{2}\frac{qB}{m}\Big\{\sqrt{(l-m)(l+m+1)}\,\delta_{m'm+1} \\
&\quad - \sqrt{(l+m)(l-m+1)}\,\delta_{m'm-1}\Big\}\delta_{l'l}\delta_{\nu'\nu} \\
&\quad - \mathrm{i}\frac{1}{\alpha}(l'm10|lm)\langle \nu l||\alpha c^{[1]}||\nu' l'\rangle \delta_{m'm}\nabla \Bigg] \\
&\quad \times F(\nu' l' m'; \boldsymbol{r}, t, \alpha) = 0\,, \\
&\quad (\nu, l) = 0, 1, 2, \ldots, \infty, \\
&\quad m = -l, -l+1, \ldots, l-1, l,
\end{aligned} \tag{14}$$

where n_0 is the neutral gas number density. The reduced matrix elements $J_{\nu\nu'}^{l}(\alpha)$, $\langle \nu l||\alpha c^{[1]}||\nu' l'\rangle$ and $\langle \nu l||K^{[1]}||\nu' l'\rangle$ of the collision operator, velocity and velocity derivative are given by (11), (12*a*) and (12*b*) of [5], respectively. For further details the reader is referred to [8].

2.2.2. Representation of the spatial dependence in the hydrodynamic regime. The treatment of the spatial dependence of the phase-space distribution function is dependent on the conditions under which the experiment is performed. As detailed above, for studies of transport in the hydrodynamic regime the spatial dependence is projected onto the number density through a (time-dependent) density gradient expansion:

$$F(\nu l m|\boldsymbol{r}, t, \alpha) = \sum_{s=0}^{\infty} \sum_{\lambda=0}^{\infty} \sum_{\mu=-\lambda}^{\lambda} F(\nu l m|s\lambda\mu; t, \alpha) G_{\mu}^{(s\lambda)} n(\boldsymbol{r}, t), \tag{15}$$

where $G_{\mu}^{(s\lambda)} n(\boldsymbol{r}, t)$ is the irreducible gradient tensor operator [38]. Substituting into (14) and equating coefficients of

$G_\mu^{(s\lambda)} n(\boldsymbol{r}, t)$ yields the following hierarchy of equations for the calculation of time-dependent transport coefficients:

$$\sum_{\nu'=0}^{\infty}\sum_{l'=0}^{\infty}\sum_{m'=-l'}^{l'}\Bigg[\left(\left[\frac{\mathrm{d}}{\mathrm{d}t}+R\right]\delta_{\nu\nu'}+n_0 J^l_{\nu\nu'}(\alpha)\right)\delta_{l'l}\delta_{m'm}$$
$$+\mathrm{i}\frac{qE}{m}\alpha(l'm10|lm)\langle\nu l||K^{[1]}(\alpha)||\nu' l'\rangle\delta_{m'm}$$
$$+\frac{1}{2}\frac{qB}{m}\Big\{\sqrt{(l-m)(l+m+1)}\,\delta_{m'm+1}$$
$$-\sqrt{(l+m)(l-m+1)}\,\delta_{m'm-1}\Big\}\delta_{l'l}\delta_{\nu'\nu}\Bigg]$$
$$\times F(\nu' l' m'|s\lambda\mu;t,\alpha)=X(\nu lm|s\lambda\mu)\,, \tag{16}$$

where

$$X(\nu lm|000)=0, \tag{17}$$

$$X(\nu lm|11\mu)=\sum_{\nu'=0}^{\infty}\sum_{l'=0}^{\infty}\Bigg[\left(-\frac{1}{\alpha}\right)(l'm-\mu 1\mu|lm)$$
$$\times\langle\nu l||\alpha c^{[1]}||\nu' l'\rangle F(\nu' l' m-\mu|000)\Bigg]$$
$$-\frac{(-1)^\mu}{\alpha}F(01-\mu|000)F(\nu lm|000). \tag{18}$$

Truncation of the ν and l summations to $\nu_{\max}$ and $l_{\max}$, respectively, and discretizing in time using an implicit finite difference scheme converts the hierarchy of systems of coupled differential equations into a hierarchy of coupled matrix equations. To establish the transport coefficient of interest in this paper we are required to solve the following members of the hierarchy $(s,\lambda,\mu)=(0,0,0),(1,1,0),(1,1,1)$. The lowest member is a non-linear equation when non-conservative processes are operative. Symmetry properties for the moments are used to minimize the computational requirements [24]. Solution of (16) for the moments $F(\nu lm|s\lambda\mu)$ allows calculation of all quantities of interest including the velocity distribution function. The quantities $\nu_{\max}$ and $l_{\max}$ are adjusted until some predetermined accuracy condition is achieved. The coefficients of interest in this paper for a crossed field configuration are the following.

- *Bulk* drift velocity vector components:

$$W_x=\frac{1}{\alpha}\sqrt{2}\,\mathrm{Im}\{F(011|000)\}$$
$$-\sum_{\nu=0}^{\infty}n_0 J^0_{0\nu}\sqrt{2}\,\mathrm{Im}\{F(\nu 00|111)\}, \tag{19}$$

$$W_z=-\frac{1}{\alpha}\,\mathrm{Im}\{F(010|000)\}$$
$$+\sum_{\nu=0}^{\infty}n_0 J^0_{0\nu}\sqrt{2}\,\mathrm{Im}\{F(\nu 00|110)\}\,. \tag{20}$$

- *Flux* diffusion tensor diagonal elements:

$$D_{xx}=-\frac{1}{\alpha}\Big[\mathrm{Re}\{F(011|111)\}-\mathrm{Re}\{F(01-1|111)\}\Big],$$
$$D_{yy}=-\frac{1}{\alpha}\Big[\mathrm{Re}\{F(011|111)\}+\mathrm{Re}\{F(01-1|111)\}\Big],$$
$$D_{zz}=-\frac{1}{\alpha}F(010|110).$$

The terms involving the summations in the bulk drift velocity represent the explicit effects of non-conservative collisions on the bulk drift velocity discussed previously. Those parts of expressions (19) and (20) not involving the summations are the respective flux drift velocity components. Note Re{} and Im{}, respectively, represent the real and imaginary parts of the moments. Expressions for mean energy ε and gradient energy parameter γ defined by a density gradient expansion of the average energy $\epsilon(\boldsymbol{r},t)=\varepsilon(t)+(\gamma(t)/n)\cdot\nabla n$ are available in [8].

2.3. Monte Carlo simulation technique

Another method for investigating swarm particle transport in neutral gases is a Monte Carlo simulation technique. For the purpose of developing simulation presented here, it is assumed that a swarm develops under the influence of spatially uniform electric and magnetic fields in an infinite space. Electrons gain the energy from the external electric field and dissipate it through collisional transfer to the neutral gas molecules by elastic and different types of inelastic collisions including the non-conservative collisions (e.g. impact ionization and attachment). Thermal motion of the background neutral particles is neglected and all simulations are performed for the low space-charge limit according to the standard definition of charged particle swarms outlined in the introduction of this work. The code has been verified for a number of benchmarks [39] which prove the accuracy and the correctness of the code.

In the context of relaxation studies, the following scenario is applied. At the time $t=0$, swarm particles are released from the origin with an initial Maxwellian velocity distribution having the mean energy of 1 eV. They continue their motion under the influence of an electric field only. After relaxation to the steady state in which both the swarm transport parameters and the distribution function do not change in time, the magnetic field is applied and the relaxation process is followed accurately in time. An extremely large number of swarm particles (typically 10^7) has been followed in a neutral gas in order to retain the good statistics of the final data, particularly the diffusion coefficients.

Temporal variation of the various transport coefficients with the field frequency and electric/magnetic field amplitude has been studied using a similar but not identical scenario. Electrons are released from the origin with the Maxwellian velocity distribution and with the mean starting energy of 1 eV under the influence of both the rf electric and magnetic fields. Transport coefficients are determined after relaxation to the steady state. The period of the field oscillations is divided by 400 (in order to meet the same resolution of the data given by the Boltzmann equation analysis and in order to have good representation of the changing fields) and these moments are also used to sample the transport coefficients.

In both scenarios we follow the evolution of each swarm particle through time steps determined by the mean collision time, the cyclotron period and period of the field. These finite time steps are used to solve the integral equation for the collision probability in order to determine the time of the next collision. This can be done using either the null-collision

method [40] or the so-called direct integration method [41]. In our code, the latter approach is employed. The number of time steps is determined in such a way as to optimize the performance of the Monte Carlo code without reducing the accuracy of the final results. All dynamic properties of each swarm particle such as the position, velocity and energy are updated between the collisions. The equations of motion are solved analytically and the reader is referred to [42] for their explicit form. Once the moment of the next collision is established, the nature of the collision is determined by using the relative probabilities of the various collision types. All swarm particle scattering is assumed to be isotropic regardless of the collision nature of specific process or energy. The definitions and corresponding formulae for the swarm particle transport coefficients were given in our previous publications [22], e.g. the flux drift velocity components and the flux diagonal elements of the diffusion tensor are given by

$$W_i = \left\langle \frac{\mathrm{d}r_i}{\mathrm{d}t} \right\rangle = \langle v_i \rangle \,, \tag{21}$$

$$D_{ii} = \langle r_i v_i \rangle - \langle r_i \rangle \langle v_i \rangle \,, \tag{22}$$

where v_i is the electron velocity and $i = x, y, z$. Most importantly, sampling of various transport properties is always performed at times fully uncorrelated with the moments of collisions.

3. Results and discussion

In this section we present results for positron and electron swarms. For positrons, we restrict our discussion to non-equilibrium transport of positrons under the influence of an electric field in gases and liquids, assessing the impact of anisotropic elastic scattering on the transport properties. For electron swarms, we consider temporal non-locality in diffusion associated with time-varying electric and magnetic fields. Electric and magnetic fields are in the z and y directions, respectively, and their strengths are presented in units of Townsends ($1\,\mathrm{Td} = 10^{-21}\,\mathrm{V\,m^2}$) and Huxley ($1\,\mathrm{Hx} = 10^{-27}\,\mathrm{T\,m^3}$).

3.1. Non-equilibrium transport of positron swarms in gases and liquids

3.1.1. Positron swarm transport in gaseous argon—impact of anisotropic elastic scattering. Recently, a complete set of cross-sections for positrons in Ar were presented and detailed in [16]. This is one of the few full sets of cross-sections available for swarm calculations. The set of cross-sections contain elastic, excitation, ionization as well as the functional Ps-formation processes and are shown in figure 1. All scattering processes were assumed to be isotropic. In this study, we extend their work to examine the impact of the anisotropic nature of the elastic differential cross-section for positrons in argon using results of a new relativistic polarized-orbital calculation which includes an *ab initio* optical potential [43, 44]. The real part of this complex optical potential describes the polarization interaction while the imaginary

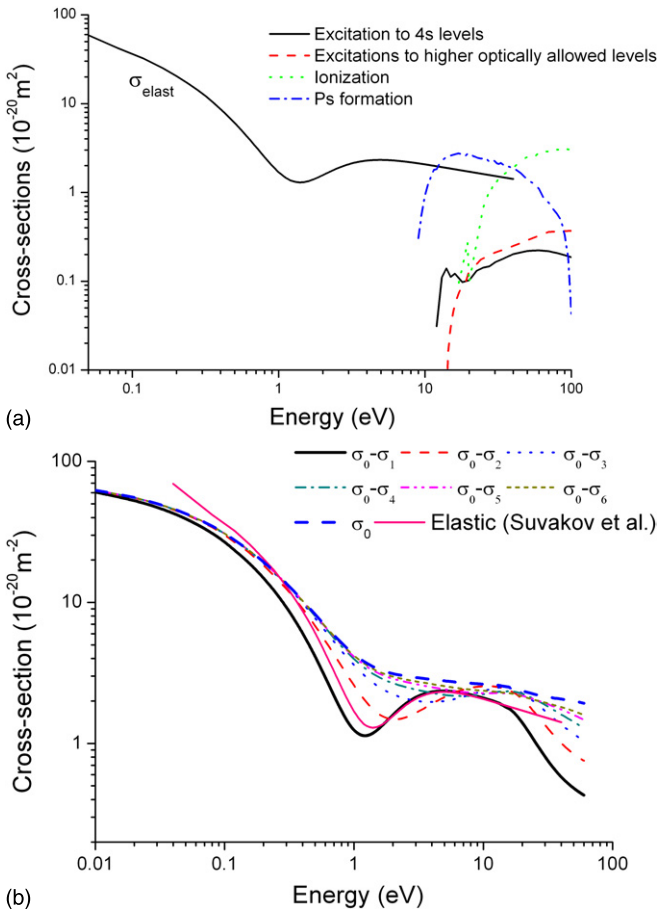

Figure 1. (*a*) Isotropic cross-sections for elastic, inelastic, Ps-formation and ionization for positrons in dilute gaseous Ar (see [16] and references therein) (*b*) Elastic partial cross-sections (23) representing the anisotropic nature of the elastic differential scattering cross-section [43, 44].

part accounts for the loss of flux from the elastic channel to those inelastic channels which are accessible at a particular energy. For implementation in the multi-term solution of the Boltzmann equation, we consider the 'partial' cross-sections defined by

$$\sigma_l(c) = 2\pi \int_{-1}^{1} \sigma(c, \chi) P_l(\cos\chi)\, \mathrm{d}(\cos\chi), \tag{23}$$

where χ is the scattering angle and P_l is a Legendre polynomial. We note that the quantity σ_0 is the total cross-section, while $\sigma_0 - \sigma_1$ is the momentum transfer cross-section σ_m. If scattering is isotropic then $\sigma_l = 0$ for $l \neq 0$. In multi-term solutions of the Boltzmann equation, these partial cross-sections occur in the combination of $\sigma_0 - \sigma_l$, where l ranges from 0 to l_max. The first few sets of these partial cross-section combinations are shown in figure 1. For comparison, the elastic cross-section used in [16] is also included.

In this section we study the impact of anisotropic elastic scattering on the transport of positrons in dilute gaseous argon at a temperature of 85 K. We present results from a multi-term solution of Boltzmann's equation for positrons in dilute gaseous argon and compare them where possible with those from the original independent Monte Carlo simulation and

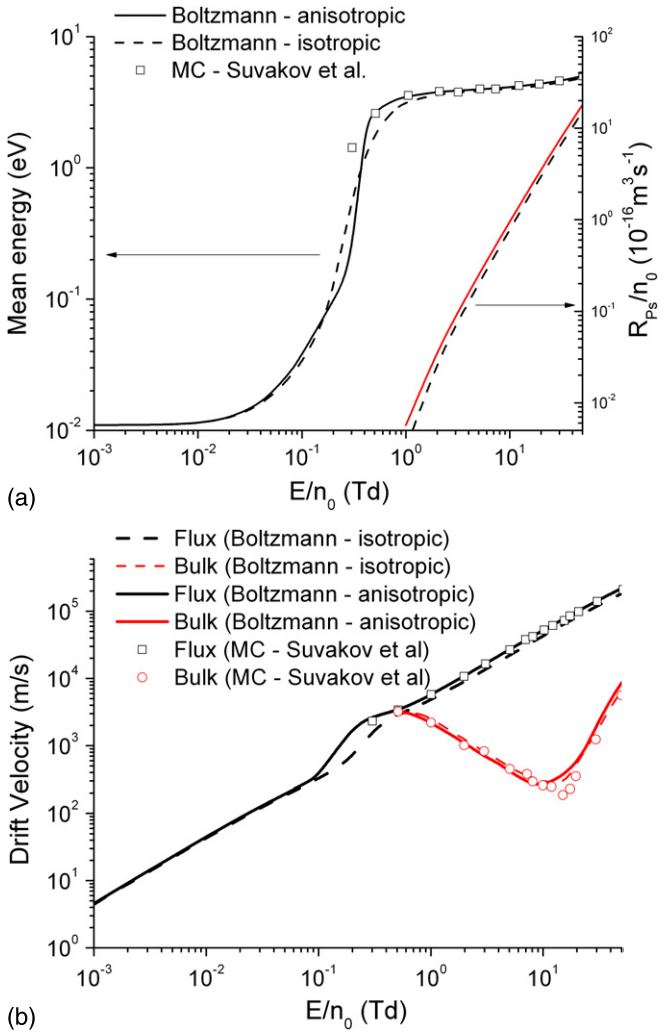

Figure 2. The variation with E/n_0 of mean energy ε and Ps-formation rates R_{Ps}/n_0, bulk and drift velocities, for positrons in dilute gaseous Ar at 85 K. These results are compared where possible with the dilute gas-phase results using Monte Carlo simulation [16].

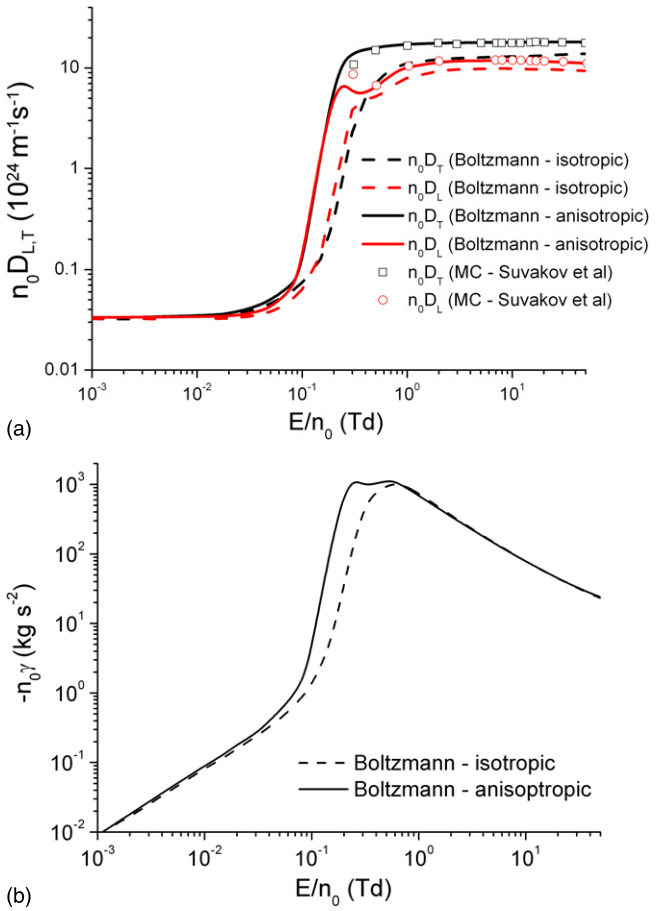

Figure 3. The variation with E/n_0 of flux diffusion coefficients (D_L and D_T represent diffusion parallel and perpendicular to the electric field, respectively), and gradient energy parameter γ for positrons in dilute gaseous Ar at 85 K. These results are compared where possible with the dilute gas-phase results using Monte Carlo simulation [16].

cross-section set [16]. In figures 2 and 3, the comparisons are made between transport properties calculated using isotropic elastic scattering and those using full anisotropic elastic scattering. The differences between the two sets are quite large, particularly in the electric field range from 0.1 to 1 Td. In this region of electric fields, the mean energy of the swarm is in the vicinity of the Ramsauer minimum and it is here where the differences between the momentum transfer (and higher order) cross-section and the total cross-section are the largest. These differences are masked somewhat by virtue of the logarithmic scale. Perhaps the most sensitive coefficients to anisotropic scattering processes are the flux diffusion coefficients shown in figure 3. For a given E/n_0 in this range, differences can be greater than an order of magnitude. This is, however, merely a shift in the profiles of a quantity that varies rapidly with E/n_0. Qualitatively, however, all features remain very similar.

In figure 2 we focus on the comparative study of the bulk and flux drift velocities and note that qualitatively there are no differences in the profiles. Most importantly, the positronium-induced negative differential conductivity (Ps-induced NDC), first predicted in [16] and independently verified in [19], is again present indicating that the phenomenon is not particularly sensitive to small variations in the anisotropic nature of elastic scattering. Quantitatively, as expected, the flux drift velocity for anisotropic scattering is greater than for isotropic scattering for all fields. We note that convergence in the bulk drift velocity for the Boltzmann equation technique is quite poor particularly in the minimum of the NDC region and consequently we are unable to definitely quantify the impact of the anisotropic nature of the elastic scattering in this region. The differences between the bulk and flux drift velocity and the origin of Ps-induced NDC are well known [16]. The bulk drift velocity is the time rate of change of the centre of mass of the swarm of positrons. It is composed of the flux drift velocity (mean velocity of positrons) plus a contribution brought about by the spatially asymmetric loss of positrons from the swarm to Ps-formation ($S^{(1)}$). This process is dependent on the Ps-formation rate and on the degree of spatial asymmetry in the average energy profile through the swarm, a (first order) measure of which is given by the gradient energy parameter γ [45] shown in figure 3. On average the positrons at the front of the swarm are more energetic than those at the trailing edge and hence there is a preferential loss of positrons to

Ps-formation at the front of the swarm as compared with the back of the swarm. This results in a shift in the centre of mass of the swarm in the opposite direction to the field force direction and consequently the bulk drift velocity is less than the flux drift velocity as shown. The strength of the Ps-formation processes and the asymmetric spatial variation of energy within the swarm in this field range is such that NDC results in the region between 0.5 and 15 Td. Physically, one may question why the flux drift velocity approaches the bulk drift velocity again given that the Ps-formation rate is increasing. We note from figure 3 in this region excitation and ionization processes begin to dominate and the energy variation through the swarm then begins to decrease. Consequently, the motion of the centre of mass due to positron loss to Ps-formation is then reduced and the bulk and flux begin to approach each other. Indications from MC simulations are that the shape of the swarm pulse can deviate significantly from a Gaussian, and in such a case non-hydrodynamic arguments may apply.

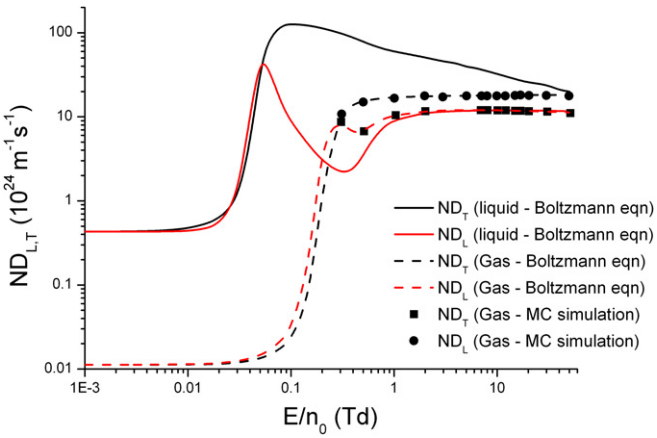

Figure 4. The variation of the flux diffusion coefficients (D_L and D_T represent diffusion parallel and perpendicular to the electric field, respectively) with E/n_0 for positrons in dilute gaseous and liquid Ar at 85 K.

3.1.2. Positron swarms in liquid argon. Cohen and Lekner [47] recognized over 40 years ago that electron transport in liquids is significantly affected by interference effects arising from coherent elastic scattering. Recently, the somewhat heuristic Cohen–Lekner two-term kinetic theory has been generalized and a multi-term solution of Boltzmann's equation is now available for both electrons and positrons in structured matter [19]. Coherent scattering effects become important when the de Broglie wavelength of the particle is comparable to or greater than the average interparticle spacing, as is the case for low energy positrons or electrons in condensed matter, and the particle wave is effectively diffracted by a number of constituent molecules. On the other hand, gases at normal temperatures and pressures (hereafter referred to as the dilute gas-phase limit) are sufficiently dilute so that the de Broglie wavelength is much smaller than the average intermolecular spacing $n_0^{1/3}$, the wave properties of the particle are suppressed, and scattering is effectively from only one gaseous molecule at a time. Physically speaking, the two situations may be likened to the diffraction and interference effects studied in physical optics, and ray tracing in geometrical optics, respectively.

These effects are accounted for quantitatively in the Boltzmann equation by combining the differential cross-section for single, elastic scattering with the dynamic structure factor [46, 47] (the temporal and spatial Fourier transform of the Van Hove pair correlation function [46]). Specifically, the partial cross-sections for exchange of momentum and higher order tensor properties are modified by a multiplicative factor equal to the static structure factor of the material. Pursuing the physical optics analogy a little further in the context of a multi-slit experiment, one recalls that the overall pattern derives from a superposition of the interference pattern of the combined slits with the diffraction pattern of each slit. The former corresponds to the static structure factor and the latter to the single scattering cross section.

For positrons in liquid argon, coherent elastic scattering produces a number of interesting effects, the most noteworthy being the existence of structure-induced NDC [19]. This effect is additional to and distinct from the Ps-formation-induced NDC which is observed for both dilute gases [16] and liquids [19]. In what follows, for the first time we present results for diffusion of positrons in liquid argon at 85 K, based on the cross-section set of [16] and the structure factor for liquid argon of [48]. The results are displayed in figure 4. The magnitudes of the diffusion coefficients of positrons in liquid argon at low fields (thermal values) are at least an order of magnitude greater for a liquid than for a dilute gas. In the high field (high energy) limit, the positron de Broglie wavelengths decrease, coherent scattering becomes less important and the liquid-phase and dilute gas-phase results converge. It is noteworthy that the degree of anisotropic diffusion, as reflected in the disparity between the longitudinal and transverse diffusion coefficients, can be much larger in liquids than in gases. Thus we see from figure 4 that the difference can be up to almost two orders of magnitude for liquids, another marked manifestation of the effects of coherent scattering.

3.2. Electron swarms and temporal non-locality

As detailed in section 1, one of the key tasks of swarm transport physics in low-temperature plasma physics is the provision of benchmarks for plasma models/simulations (or components thereof) in the swarm limit. In addition, such benchmarks provide an indication as to the sensitivity of transport to variations in the various parameters available to the system. Recently, a benchmark model simulating field conditions in the bulk of an inductively coupled plasma was presented by the Petrović group using a Monte Carlo simulation [21]. The model unearthed a multitude of interesting phenomena for diffusion including the existence of transient negative diagonal diffusion elements. The focus of this section is to benchmark the current time-dependent multi-term solution of Boltzmann's equation against time-resolved Monte Carlo technique for the model presented in [21]. Initially we will focus on the temporal relaxation of diffusion coefficients in E and B fields and then

study the manifestations of these on the time-resolved profiles under rf electric and magnetic fields[4].

3.2.1. Transient response of electrons in E and B fields. In a recent paper [50], the transient response of electron swarms to the application of an orthogonal magnetic field was considered. The initial condition is a steady-state distribution for a dc electric field only ($E/n_0 = 12$ Td, $B/n_0 = 0$ Hx). At time t=0, a crossed magnetic field is switched on (electric field is unaltered) and the relaxation properties of the swarm are monitored as a function of the density normalized time, $n_0 t$. The influence of the magnetic field on the transient response of the diffusion coefficients calculated using the multi-term solution of Boltzmann's equation is displayed in figure 5 where they are compared with results from a MC simulation. The excellent agreement between these two independent methods validates the basis of transport phenomena as well as numerical integrity of both the Boltzmann and the Monte Carlo codes.

In the relaxation profiles we observe the existence of three distinct timescales: (i) the gyro-period of the electrons τ, (ii) the momentum relaxation time τ_m and (iii) the energy relaxation time τ_e. The latter two timescales are functions of energy. The various diffusion coefficients display profiles that are either essentially monotonic or damped periodic relaxation. For diffusion along the B-field direction ($n_0 D_{yy}$) relaxation is in general always non-periodic since there is no explicit B-field effects in this direction, and relaxation occurs on the timescale governed by τ_e. In contrast, the relaxation profiles of diffusion coefficients in the $\boldsymbol{E}$($n_0 D_{zz}$) and $\boldsymbol{E} \times \boldsymbol{B}$ ($n_0 D_{xx}$) directions exhibit a transition from monotonic decay to damped periodic decay as the magnetic field strength is increased to values where $\tau \leqslant \tau_m$. For the damped periodic profiles, the oscillations are on the timescale of the gyro-orbits τ and the envelope decays on a timescale of τ_m together with a further relaxation on the timescale of τ_e. The existence of the additional oscillatory behaviour in the relaxation profiles is an imprint of the collective gyrations of the ensemble of electrons damped by collisions that exchange momentum and energy. Perhaps the most interesting phenomenon is the existence of transiently negative excursions of the diffusion tensor elements in both the $\boldsymbol{E}$ and $\boldsymbol{E} \times \boldsymbol{B}$ directions. A physical discussion of this phenomenon is detailed in [50].

The manifestations of these complex relaxation profiles for time-dependent fields (e.g. rf and/or pulsed rf) result in behaviour which is distinctly non-local in time as we now demonstrate.

3.2.2. Rf electric and magnetic fields. In this section we consider the benchmark model for electron swarms in rf electric and magnetic fields proposed by Raspopovic *et al* [21]. The Reid ramp model is again employed with orthogonal, spatially homogeneous fields that are $\pi/2$ out of phase ($E/n_0 = 10\sqrt{2}\sin(\omega t)$ Td, $B/n_0 = 500\cos(\omega t)$ Hx, where ω is the angular field frequency). The neutral gas density is fixed at $n_0 = 3.54 \times 10^{22}$ m^{-3}. In figure 6 we display the diagonal components of the diffusion tensor in the periodic steady state as a function of the field phase for various applied frequencies of the field. Once again there is very good agreement between

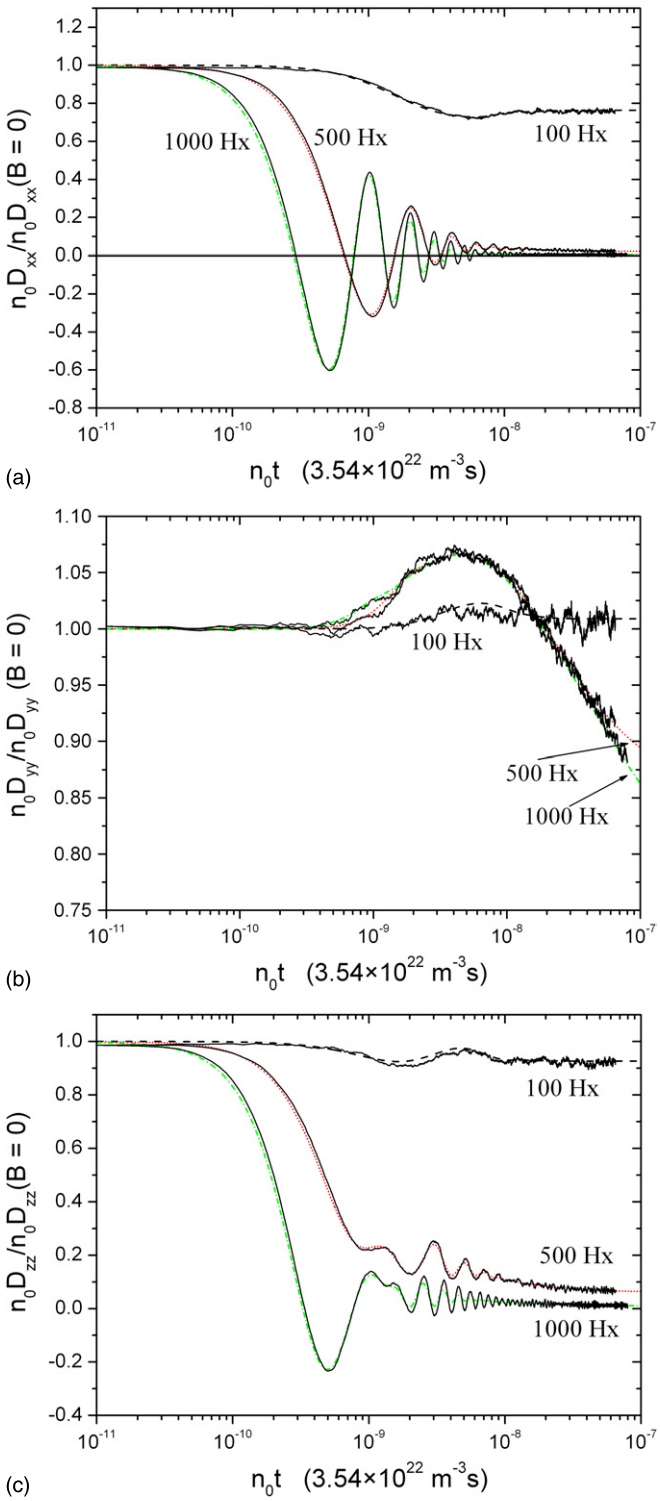

Figure 5. Temporal relaxation of the diagonal elements of the diffusion tensor D_{xx}, D_{yy} and D_{zz} for various applied magnetic fields in a crossed field configuration for Reid ramp model (dashed lines: Multi-term Boltzmann solution; thin lines: Monte Carlo code).

[4] We implement in this study the well-known benchmark Reid ramp model [49], used for a variety of field configurations previously due to its well-known failure of the two-term approximation [5].

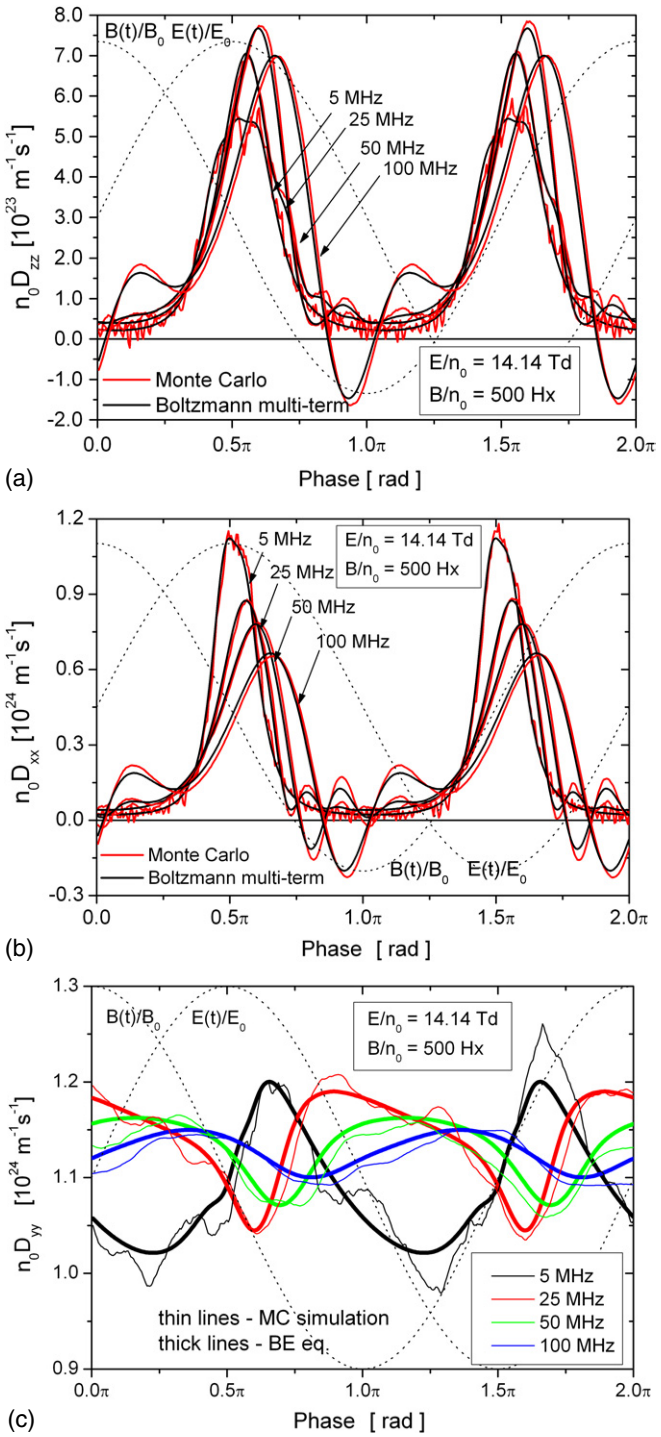

Figure 6. Comparison of the multi-term Boltzmann solution and Monte Carlo results for $n_0 D_{zz}$, $n_0 D_{xx}$ and $n_0 D_{yy}$ over a range of applied field frequencies for the Reid ramp model.

the two independent techniques, further supporting the validity of both techniques. Large scatter in diffusion data at low frequency and for $n_0 D_{yy}$ obtained in Monte Carlo simulations is the result of poor statistics which requires following a large number of electrons and their complete relaxation.

There are some anomalous features in these profiles [8, 21]. The behaviour demonstrated for the diffusion in the $\boldsymbol{E}$ and $\boldsymbol{E} \times \boldsymbol{B}$ directions is in general not predictable from steady-state dc results [23, 51]. Contemporary understanding of field frequency effects (namely reduction in amplitude and increase in phase-lag with respect to the field) fails or has a limited range of validity when the relaxation is not monotonic. Understanding such effects requires recourse to a systematic investigation of relaxation profiles: '*one must consider not only the ability of the transport property to relax on a time scale governed by the frequency of the field but also the implications associated with an inability to relax*' [52]. At low-frequencies, the time available for relaxation before the field changes is high and we essentially sample the long-time behaviour of the relaxation profiles in figure 5. The quasi-dc behaviour then follows, which has no additional (higher order) oscillatory behaviour present in the rf profiles. As we increase the frequency, however, the time available for relaxation before the field changes decreases and we begin to sample complex oscillatory behaviour in the relaxation profiles of figure 5. The additional (high order) oscillatory behaviour in the rf profiles then follows. Using similar arguments one can understand the transient negative excursions of $n_0 D_{xx}$ and $n_0 D_{zz}$ above a certain frequency (and B/n_0), the enhancement of the peak value of $n_0 D_{yy}$ and its transition to anti-phase behaviour as as ω/n_0 increases.

4. Conclusion

Swarm physics is alive! Accurate swarm transport theories, developed in the 1970–1990s to unfold swarm experiments, have now been adapted and find application in a variety of fields. In this paper we have highlighted their application in the field of low-temperature plasmas and positron physics. For low-temperature plasmas, we have presented a benchmark simulation of electron swarms under the action of crossed rf electric and magnetic fields. The results of a time-dependent multi-term solution of Boltzmann's equation were compared with those of an independent Monte Carlo simulation, with very good agreement. For positron swarms, we highlighted the sensitivity of the macroscopic transport properties to the anisotropic nature of elastic scattering for positrons in gaseous argon. The extension to consider positrons in liquid argon demonstrated an enhancement of the anisotropic nature of diffusion over the dilute gas phase.

Acknowledgments

All the authors would like to acknowledge the support of the Australian Research Council and the Centre for Antimatter-Matter Studies. This research is also funded in part by the MNTRS project 141025 (SD, ZLjP).

References

[1] Huxley L G H and Crompton R W 1974 *The Drift and Diffusion of Electrons in Gases* (New York: Wiley)
[2] Crompton R W 1994 *Adv. At. Mol. Opt. Phys.* **32** 97
[3] Petrović Z Lj, Šuvakov M, Nikitović Z, Dujko S, Šašić O, Jovanović J, Malović G and Stojanović V 2007 *Plasma Sources Sci. Technol.* **16** S1

[4] Petrović Z Lj, Raspopović Z M, Stojanović V D, Jovanović J V, Malović G, Makabe T and de Urquijo J 2007 *Appl. Surf. Sci.* **253** 6619
[5] Ness K F and Robson R E 1986 *Phys. Rev.* A **34** 2185
[6] Allis W P 1956 *Handbuch der Physik* vol 21 (Berlin: Springer)
[7] Winkler R, Loffhagen D and Sigeneger F 2002 *Appl. Surf. Sci.* **192** 50–71
[8] White R D, Ness K F and Robson R E 2002 *Appl. Surf. Sci.* **192** 26–49
[9] Robson R E, White R D and Petrović Z Lj 2005 *Rev. Mod. Phys.* **77** 1303–20
[10] Petrović Z Lj, Raspopović Z M, Dujko S and Makabe T 2002 *Appl. Surf. Sci.* **192** 1–21
[11] Cherry S R, Sorensen J A and Phelps M E 2003 *Physics in Nuclear Medicine* (Philadelphia, PA: Saunders)
[12] Surko C M, Gribakin G F and Buckman S J 2005 *J. Phys. B: At. Mol. Opt. Phys.* **38** R57–126
[13] Sullivan J P, Makochekanwa C, Jones A, Caradonna P and Buckman S J 2008 *J. Phys. B: At. Mol. Opt. Phys.* **41** 081001
[14] Mitroy J and Bromley M W J 2007 *Phys. Rev. Lett.* **98** 173001
[15] Kadyrov A S, Bray I and Stelbovics A T 2007 *Phys. Rev. Lett.* **98** 263202
[16] Suvakov M, Petrovic Z L, Marler J P, Buckman S J, Robson R E and Malovic G 2008 *New J. Phys.* **10** 053034
[17] Bankovic A, Marler J P, Suvakov M, Malovic G and Petrovic Z L 2008 *Nucl. Instrum. Methods Phys. Res. Sect. B-Beam Interact. Mater. At.* **266** 462
[18] Sullivan J P, Buckman S J, Jones A, Caradonna P, Makochekanwa C, Slaughter D, Petrović Z Lj, Banković A, Dujko S, Marler J P and White R D 2009 *J. Phys. Conf. Ser.* **162** 012002
[19] White R D and Robson R E 2009 Positron kinetics in soft condensed matter *Phys. Rev. Lett.* **102** 230602
[20] Bzenić S, Raspopović Z M, Sakadžić S and Petrović Z Lj 1999 *IEEE. Trans. Plasma Sci.* **27** 78
[21] Raspopović Z, Sakadžić S, Petrović Z Lj and Makabe T 2000 *J. Phys. D: Appl. Phys.* **33** 1298
[22] Dujko S, White R D, Ness K F, Petrović Z Lj and Robson R E 2006 *J. Phys. D: Appl. Phys.* **39** 4788
[23] Ness K F 1994 *J. Phys. D: Appl. Phys.* **27** 1848
[24] White R D, Ness K F, Robson R E and Li B 1999 *Phys. Rev.* E **60** 2231
[25] White R D, Robson R E and Ness K F 1999 *Phys. Rev.* E **60** 7457
[26] Li B, White R D, Robson R E and Ness K F 2001 *Ann. Phys.* **292** 179–98
[27] Li B, Robson R E and White R D 2006 *Phys. Rev.* E **74** 026405
[28] Loffhagen D and Winkler R 1996 *J. Phys. D: Appl. Phys.* **29** 618
[29] Winkler R 2000 *Adv. At. Mol. Opt. Phys.* **43** 19
[30] Maeda K, Makabe T, Nakano N, Bzenić S and Petrović Z Lj 1997 *Phys. Rev.* E **55** 5901
[31] Shimada T, Nakamura Y, Petrović Z Lj and Makabe T 2003 *J. Phys. D: Appl. Phys.* **36** 1936
[32] Trunec D, Bonaventura Z and Necas D 2006 Solution of the time-dependent boltzmann equation for electrons in non-thermal plasma *J. Phys. D: Appl. Phys.* **39** 2544–52
[33] Makabe T and Petrović Z Lj 2006 *Plasma Electronics: Applications to Microelectronic Device Fabrication* (New York: Taylor and Francis)
[34] Kumar K, Skullerud H R and Robson R E 1980 *Aust. J. Phys.* **33** 343
[35] Tagashira H, Sakai Y and Sakamoto S 1977 *J. Phys. D: Appl. Phys.* **10** 1051
[36] Boltzmann L 1872 *Wein. Ber.* **66** 275
[37] Wang-Chang C S, Uhlenbeck G E and De Boer J 1964 *Studies in Statistical Mechanics* vol 2 ed J De Boer and G E Uhlenbeck (Wiley: New York) p 241
[38] Robson R E and Ness K F 1986 *Phys. Rev.* A **33** 2068
[39] Raspopović Z M, Sakadžić S, Bzenić S A and Petrović Z Lj 1999 *IEEE Plasma Sci.* **27** 1241
[40] Skullerud H R 1968 *J. Phys. D: Appl. Phys.* **1** 1567
[41] Itoh H and Musha T 1960 *J. Phys. Soc. Japan* **15** 1675
[42] Biagi S F 1999 *Nucl. Instrum. Methods* A **421** 234
[43] Chen S, McEachran R P and Stauffer A D 2008 *J. Phys. B: At. Mol. Opt. Phys.* **41** 025201
[44] McEachran R P and Stauffer A D 2009 *J. Phys. B: At. Mol. Opt. Phys.* **42** 075202
[45] White R D, Robson R E and Ness K F 1995 *Aust. J. Phys.* **48** 925
[46] Van Hove L 1954 *Phys. Rev.* **95** 249–62
[47] Cohen M H and Lekner J 1967 *Phys. Rev.* **158** 305–9
[48] Yarnell J L, Katz M J, Wenzel R G and Koenig S H 1973 *Phys. Rev.* A **7** 2130–44
[49] Reid I D 1979 *Aust. J. Phys.* **32** 231
[50] White R D, Dujko S, Ness K F, Robson R E, Raspopović Z M and Petrović Z Lj 2008 *J. Phys. D: Appl. Phys.* **41** 025206
[51] White R D, Brennan M J and Ness K F 1997 *J. Phys. D: Appl. Phys.* **30** 810–6
[52] White R D 2001 *Phys. Rev.* E **64** 056409